Localization of the Binding Site for Modified Gb_3 on Verotoxin 1 Using Fluorescence Analysis†

William D. Picking,*,‡ Jameson A. McCann,‡ Anita Nutikka,§ and Clifford A. Lingwood§

Department of Biology, Saint Louis University, 3507 Laclede Avenue, St. Louis, Missouri 63103, Department of Microbiology, Research Institute, Hospital for Sick Children, Toronto, Ontario M5G 1X8, Canada, and Departments of Clinical Biochemistry, Biochemistry and Microbiology, University of Toronto, Toronto, Ontario, Canada

Received September 29, 1998; Revised Manuscript Received April 5, 1999

ABSTRACT: Verotoxins (VTs) from *Escherichia coli* elicit human vascular disease as a consequence of specific binding to globotriaosylceramide (Gb_3) receptors on endothelial cell surfaces. Molecular models based on the VT1 crystal structure were used previously to investigate the structural basis for receptor recognition by VT1 and other verotoxins. Interestingly, these model-based predictions of glycolipid binding to VT1 differ somewhat from recently published structural data from cocrystals of the VT1 B-subunit (VT1B) and an analogue of the sugar moiety of Gb_3. In this study, fluorescence spectroscopy was used to test model-based predictions of the location of Gb_3 binding on the B-subunit pentamer of VT1. Resonance energy transfer was used to calculate the distance from a coumarin probe used to replace the acyl tail of Gb_3 and the single tryptophan residue (Trp34) present within each VT1B monomer. The observed energy transfer efficiency (greater than 95%) suggests that these two moieties are approximately 13.3 Å apart when a single distance is assumed. This distance is consistent with proposed models for the fit of Gb_3 within the "cleft site" of the VT1 B-subunit. When the distances from Trp34 to the other coumarinGb_3 molecules (bound to each of the four remaining monomers within the VT1B pentamer) are taken into consideration, it appears likely that the coumarin-modified Gb_3 analogue used in this study associates with the previously proposed receptor binding site II of VT1. This is consistent with an observed binding preference of VT2c for coumarinGb_3. To provide additional information on the association of Gb_3 with the VT1 B-subunit, the influence of Gb_3 glycolipid binding on the accessibility of Trp34 to different quenching agents in solution was then examined. Taken together, the data suggest that coumarin-labeled Gb_3 preferentially binds to site II on VT1 in a position that is consistent with the previously described molecular models.

Verotoxins (VTs)[1] are *Escherichia coli* subunit toxins composed of a single ~30 kDa A-subunit and five noncovalently associated 7.5 kDa B-subunits. After entering the cytoplasm, VTA blocks protein synthesis in eukaryotic cells as a result of an *N*-glycanase activity that targets 28S ribosomal RNA (*1*). The role of the B-subunit in cellular intoxication is to direct the VT1 holotoxin to specific target cell populations by virtue of its receptor binding properties (*2, 3*). Members of the verotoxin family are responsible for microvascular disorders such as hemorrhagic colitis and hemolytic uremic syndrome (HUS) (*4*) as a result of specifically affecting cells that express the appropriate cell-surface globotriaosylceramide receptors (Gb_3; Galα1−4Galβ1−4Glc ceramide). HUS in children follows gastrointestinal infection with VT-producing *E. coli*. This illness can be devastating to the very young with effects that correlate with selective expression of Gb_3 in the renal glomeruli of children (*5*), suggesting an epidemiology that is largely determined by receptor distribution (*6*).

Cultured endothelial cells provide an effective model for studying the effects of verotoxin (*7, 8*) whose sensitivity to the toxin can be modulated by cytokine treatment (*9, 10*). The VT1 receptor, Gb_3, also acts as a human B-cell differentiation antigen (*11, 12*) which is involved in signal transduction through the α_2-interferon receptor (*13*−*15*) and CD19 (*16*). Each of these proteins contains a domain resembling that of the Gb_3 binding VT1 B-subunit (VT1B) (*17, 18*). VTB association with Gb_3 on B-lymphocytes induces apoptosis in these cells (*19*), and VT is able to block B cell function in vitro (*20*). Interestingly, enhanced Gb_3 synthesis in some human tumors renders them highly sensitive to killing by VT1 in vitro and in vivo (*21*). Therefore, knowledge of the molecular basis for Gb_3 binding by VT1B will be extremely useful in designing strategies to

†This work was supported by a grant from the Medical Research Council of Canada to C.A.L. and a Saint Louis University Summer Research Award to W.D.P.

* Corresponding author. Telephone: (314) 977-3912. FAX: (314) 977-3658. Email: pickinwd@slu.edu.

‡ Saint Louis University.

§ Hospital for Sick Children and University of Toronto.

[1] Abbreviations: HUS, hemolytic uremic syndrome; VT, verotoxin; VT1, verotoxin 1; VT1B, B-subunit homopentamer of VT1; Gb_3, globotriaosylceramide; Pk-MCO, αGal(1−4)βGal(1−4)BGlc(1−8)-methoxycarbonyloctyl; Trp34, single tryptophan residue of VT1B; lysoGb_3, Gb_3 lacking an acyl group on its ceramide moiety; coumarinGb_3, lysoGb_3 labeled with coumarin-3-carboxylic acid; PC, phosphatidylcholine; RET, resonance energy transfer; K_{SV}, Stern−Volmer steady-state quenching constant; MV^{2+}, methyl viologen.

10.1021/bi982335n CCC: $18.00
Published on Web 05/14/1999

combat human vascular disease, understand B-cell differentiation, and develop effective new neoplastic therapies.

A combination of theoretical calculation and experimental binding studies has been useful in predicting the location of the Gb_3 binding sites (*22*, *23*) within the known crystal structure of VT1B (*24*). Unfortunately, these studies are not in complete agreement with recently published crystal structure data on complexes composed of VT1B and the Gb_3 analogue 8-(methoxycarbonyl)octyl trisaccharide (Pk-MCO) (*25*). Here we show that a fluorescent derivative of Gb_3 possessing a coumarin probe in place of the acyl group normally attached to the Gb_3 ceramide moiety is useful for monitoring interactions between VT1B and its receptor. In particular, this Gb_3 derivative is useful for providing new information on the position of the Gb_3 binding site within VT1B relative to the position of the single tryptophan residue (Trp34) present within each VT1B monomer. Additional data from the quenching of Trp34 fluorescence are also presented which support model-based predictions concerning the physical nature of the Gb_3−VT1B interface following receptor−ligand association.

MATERIALS AND METHODS

Materials. Sodium iodide, 1,1′-dimethyl-4,4′-bipyridinium (methyl viologen or MV^{2+}), and Gb_3 were purchased from Sigma Chemical Co. Tris buffer and acrylamide were from Fisher Scientific (St. Louis, MO). Recombinant VT1 was purified and lyso-Gb_3 prepared from Gb_3 as previously described (*26*). Coumarin-3-carboxylic acid was from Fluka. Pyridine and *N*,*N*′-dicyclohexylcarbodiimide (DCC) were from Pierce (Rockford, IL).

Preparation of Fluorescent Gb_3. Coumarincarboxylic acid was dissolved in pyridine. An equimolar amount of DCC was added to the mixture, which was then incubated 10 min at room temperature. LysoGb_3 (1:10 molar ratio with the carboxylic acid) dissolved in pyridine was added to the activated carboxylic acid, and the entire reaction mixture was incubated overnight at room temperature. The reaction mixture was then dried under nitrogen and treated with 1 N NaOH in methanol overnight at room temperature to remove coumarin label that had reacted with the hydroxyl groups on the carbohydrate portion of Gb_3. The saponification reaction was neutralized and unreacted lysoGb_3 removed by silica column chromatography using chloroform/methanol/water (65:25:4). Reaction products were monitored by thin-layer chromatography (TLC) with detection by UV light analysis or orcinol staining. For use in fluorescence experiments, coumarinGb_3 was dissolved in methanol to a final concentration of 100 μM which was determined based on its absorbance maximum at 300 nm. Verotoxin (VT1a and VT2c) binding to glycolipids was determined using a TLC overlay assay as previously described (*27*).

Glycolipids (fluorescent or nonfluorescent) were added directly to preformed small unilamellar vesicles generated using phosphatidylcholine (PC) as described previously (*28*). Briefly, 1 mg of PC was dried and suspended in 1 mL of 20 mM Tris-HCl (pH 7.5), 150 mM NaCl (TBS) by sonication. Liposomes were allowed to form spontaneously by incubating the sample overnight at 25 °C. These vesicles were used within 3 days of their generation. The direct addition of Gb_3 and coumarinGb_3 to these vesicles allows the glycolipid to incorporate into the accessible outer face of the membranes as was previously done with ganglioside GM_1 for studying the association of the cholera toxin B subunit with its cellular receptor (*28*).

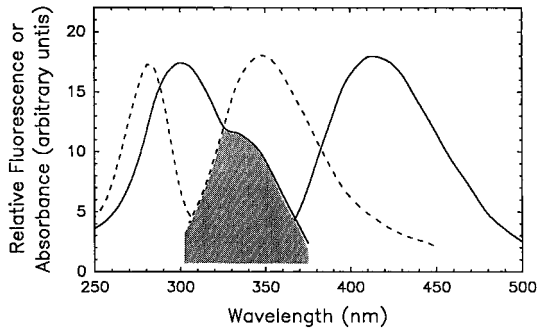

FIGURE 1: Absorption and emission spectra of Trp34 of VTB and coumarinGb_3. The left and right dashed curves show normalized absorption and emission spectra for Trp34 of VT1B (0.5 μM), respectively. Each spectrum was taken in the presence of excess Gb_3 (1 μM). The left and right solid lines show normalized absorption and emission spectra for coumarinGb_3 (1 μM), respectively. In each case, the emission spectra were obtained using an excitation wavelength equal to the maximum of sample absorbance. The shaded area shows the region of overlap for the Trp34 emission spectrum (in the presence of Gb_3) and the normalized coumarinGb_3 absorption spectrum.

Fluorescence Spectroscopy. Steady-state fluorescence analyses were carried out using a Spex (Edison, NJ) FluoroMax spectrofluorometer with a temperature-controlled sample compartment, automatic correction for the wavelength dependence of lamp intensity, automatic blank subtraction, and removable polarization filters. Trp34 fluorescence was measured using an excitation wavelength of 282 nm and with emission scanned from 300 to 400 nm. To avoid an inner filter effect, spectra were measured with a sample absorbance of less than 0.1 at both the excitation and emission wavelengths. Samples for fluorescence measurements were in a final volume of 0.6 mL and contained 20 mM Tris-HCl (pH 7.5), 150 mM NaCl, and 1 mg/mL PC as preformed vesicles. All fluorescence measurements were taken at 25 °C.

Distance Determinations Using Resonance Energy Transfer (RET). RET is the passage of excitation energy from a donor fluorophore (**d**) to an acceptor (**a**) molecule whose absorption overlaps donor emission. RET efficiency (***E***) for a given **d**−**a** pair is dependent upon three factors: (1) the overlap of the **d** emission and **a** absorption spectra (given by the spectral overlap integral *J*); (2) the relative orientation of **d** and **a** dipoles (given by κ^2 and ranging from 0 to 4); and (3) the distance separating **d** and **a**. When *J* and κ^2 are known, ***E*** is useful for calculating the distance from the **d** to **a** (*29*, *30*). Significant overlap between the emission spectrum of Trp34 and the absorption spectrum of coumarin-Gb_3 (Figure 1) makes RET a convenient method for determining the distance from the site occupied by the acyl tail of Gb_3 to Trp34 of VT1B (see *28*).

J is relatively simple to determine for a given **d**−**a** pair; however, difficulty in determining a precise κ^2 value in biological systems makes it necessary to assume a random orientation for the **d** and **a** dipoles ($\kappa^2 = {}^2/_3$). This can be a source of error in distance determinations using RET, particularly if κ^2 deviates far from a dynamically averaged value (*31*). Estimation of the uncertainty introduced by not

knowing κ^2 is possible using a variety of approaches (*31*, *32*); however, dos Remedios and Moens (*33*) present a convincing argument for using RET to determine intermolecular distances in biological systems without possessing precise knowledge of κ^2. For the distance determinations here, half-height limits of uncertainty were estimated based on the extent of isotropical randomization of **d** and **a** which can be estimated from their fluorescence anisotropy and polarization values (*31*). Fluorescence polarization data were determined as described previously (*34*), and half-height limits of uncertainty were applied according to the method of Haas and co-workers (*30*).

$\boldsymbol{E}$ is calculated from $\boldsymbol{E} = 1 - (F_{da}/F_d)$ (eq 1) where F_{da} is the fluorescence intensity of **d** in the presence of **a** and F_d is the fluorescence intensity of **d** in the absence of **a**. After determining R_0 (the theoretical distance that would give 50% $\boldsymbol{E}$) for the Trp34−coumarinGb_3 pair, the distance actually separating these two moieties was calculated from $\boldsymbol{E} = R_0^6/(R_0^6 + r^6)$ (eq 2), where r is the calculated distance between Trp34 and the probe on coumarinGb_3.

A factor that complicates RET-based distance determinations for the Trp34−coumarinGb_3 pair is the likelihood that each Trp34 donor is paired not only with the coumarin acceptor bound to its respective VT1B monomer, but also with the coumarin acceptors on adjacent monomers. When the distance separating a donor and multiple acceptors is asymmetric, the inverse sixth power relationship between $\boldsymbol{E}$ and r ensures that the acceptor nearest to each donor dominates the energy transfer process. In contrast, the presence of multiple and equidistant acceptors requires a specially modified RET analysis (*35*). From the crystal structure of VT1 and the models of Gb_3 binding being tested here, it is unlikely that the labels on two coumarinGb_3 probes are bound such that they are equidistant from Trp34, thereby preventing the need to use the modified RET analyses. From the molecular models of Gb_3 binding at sites I and II, the distances from C1 in the acyl group of bound Gb_3 (now occupied by a coumarin label) to C_γ of Trp34 on VT1B are 22.3 and 18.8 Å, respectively (*22*, *23*). In contrast, the distance from C_α of Trp34 to the C1 group on the glucose of Pk-MCO measured in cocrystals with VT1B is 23.3 Å for binding at site I and 22.6 Å for binding at site II. When these distances are considered, the anticipated distance from C_γ of Trp34 to the C1 of the acyl group (the point at which the coumarin probe is attached) should be greater than that for either of the model-based Gb_3 binding sites. Unfortunately, this distance cannot be directly measured from the cocrystal structure because the sphingosine moiety is not present in Pk-MCO. Interestingly, in the structural analysis of the VT1B/Pk-MCO cocrystals, a third potential binding site for Gb_3 was observed which places Gb_3 in intimate contact with Trp34 and places the C1 of glucose 14.4 Å from the C_α of the tryptophan. However, there are no other structural data available which corroborate the presence of a third Gb_3 binding site on VT1B (*36*), and substitution of Gly or Phe at position 34 does not have a major impact on the cytotoxicity of VT1 (*37*).

Influence of Gb_3 Binding on Solute Quenching of Trp34 Fluorescence. To monitor the influence of Gb_3 binding on the accessibility of Trp34 to interaction with solute molecules present in the aqueous environment, the sensitivity of Trp34 fluorescence to small molecular quenching agents was done according to the relationship described by Stern and Volmer (*38*). The steady-state quenching constant (K_{SV}) for Trp34 following excitation at 282 nm was determined in the absence and presence of an excess of nonfluorescent Gb_3. For each quenching agent tested, the fluorescence intensity of Trp34 was measured in the absence of quencher (F_0), and then in the presence of increasing concentrations of the quencher (F). F_0/F was then plotted as a function of the quenching agent's concentration, given by [Q], to give a linear plot whose slope gives K_{SV} according to the relationship $[Q] = 1 + F_0/F$ (eq 3) (*38*). K_{SV} values can be compromised by the presence of both diffusive (collisional) and static (ground-state complex formation) components. When curved plots were observed, diffusive and static quenching events were known to be simultaneously occurring. The initial slopes of the curved plots were used to determine K_{SV}. In the absence of extensive fluorescence lifetime data for determining specific dynamic and static quenching constant values, the implications of observing each type of quenching are discussed.

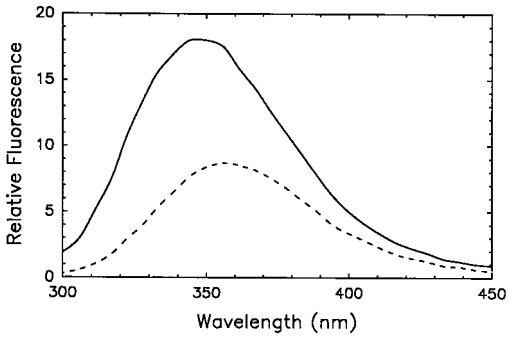

FIGURE 2: Effect of Gb_3 binding on the fluorescence of Trp34 of VT1B. Fluorescence emission spectrum of Trp34 (0.5 μM VT1B monomers) in the absence (dashed line) or presence (solid line) of approximately 1 μM Gb_3 in 10 mM sodium phosphate (pH 7.2) with 150 mM NaCl (PBS). Excitation was at 282 nm at 23 °C in a final volume of 0.6 mL.

RESULTS

Effect of Gb_3 Binding on Trp34 Fluorescence. Gb_3 binding to VT1B enhances the fluorescence of a single tryptophan residue (Trp34) present within each B-subunit monomer (Figure 2). This fluorescence enhancement is accompanied by a blue shift in the Trp34 emission spectrum (Figure 2) that is similar to the spectral shift seen in shiga toxin following association with its Gb_3 receptor (*39*). The emission maximum of VT1B is about 353 nm which shifts up to 6 nm to the blue upon interaction with Gb_3 (Figure 2). These data imply that: (1) Gb_3 binds near enough to the site occupied by Trp34 to influence the fluorescence properties of the latter; (2) Gb_3 binding induces a change in VT1B conformation that alters the fluorescence properties of Trp34; or (3) Gb_3 binding alters the physicochemical properties of the environment surrounding Trp34 to influence its fluorescence properties. To further investigate these possibilities, the distance from Trp34 to the acyl attachment site on Gb_3 was determined using resonance energy transfer (RET).

Determination of the Distance from Trp34 to the Coumarin Probe Linked to Gb_3. Because the fluorescence emission spectrum of Trp34 within the VT1B−Gb_3 complex overlaps the absorption spectrum of coumarinGb_3, RET could be used

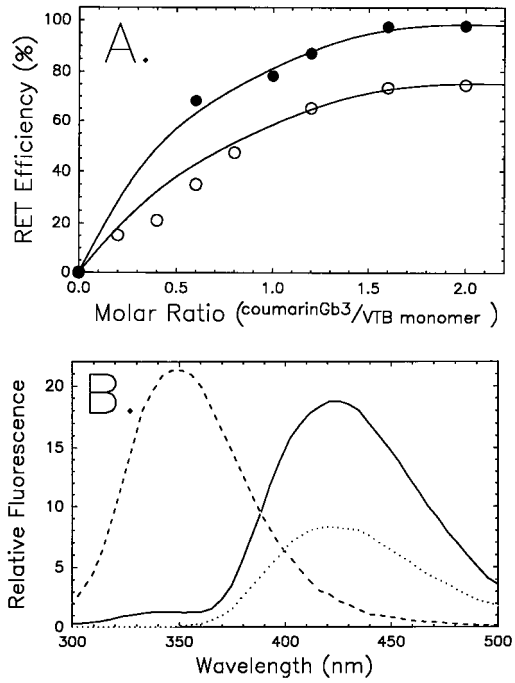

FIGURE 3: RET from Trp34 to coumarinGb_3. In (A), VT1 (open circles) or VT1B (closed circles) was added to PC vesicles into which increasing amounts of Gb_3 or coumarinGb_3 (from 0 to 1 μM) had been added so that RET efficiency could be calculated as a function of coumarinGb_3 concentration. In each case, the final concentration of VT1B monomer was 0.5 μM. The RET efficiency for VT1 with coumarinGb_3 increased almost linearly until leveling off at about 75% while the RET efficiency using VT1B leveled off at 98%. For each protein preparation, saturation of RET (as determined by a leveling off of RET efficiency as the coumarinGb_3 concentration was increased) started to occur at about a 1:1 molar ratio for VT1B and coumarinGb_3. In (B), the emission spectra are shown for VT1B (0.5 μM monomer concentration) with 1 μM Gb_3 (dashed line) or 1 μM coumarinGb_3 (solid line). The emission spectrum for VT1B with nonfluorescent Gb_3 is shown here at half-scale so that it is possible to see the size and shape of the emission spectrum of Trp34 in the presence of coumarinGb_3. The dotted line is the emission spectrum for 1 μM coumarin Gb_3 in the absence of added protein. In all cases, fluorescence excitation was at 282 nm.

to calculate the intermolecular distance separating these two fluorescent moieties. As was shown in Figure 1, the fluorescence emission maximum of Trp34 in the presence of nonfluorescent Gb_3 (at about 348 nm) provides a useful wavelength for measuring Trp34 emission without any contribution from the coumarinGb_3 emission spectrum. The spectral overlap integral (J) for this **d**−**a** pair was calculated to be 7.71×10^{-15} cm^3/M, and the R_0 distance was 25.4 Å based upon a Trp34 fluorescence quantum yield of 0.23.

When VT1B was titrated with increasing concentrations of coumarinGb_3 incorporated into PC liposomes, the RET efficiency saturated at 98% (Figure 3A). The overall shape of the Trp34 emission spectrum following RET (with an emission maximum near 345 nm) suggests that residual fluorescence is actually from Trp34 on VT1B monomers with Gb_3 bound to them (Figure 3B). Based on this RET efficiency, the distance from the coumarin probe attached to Gb_3 to Trp34 is about 13.3 Å when a single distance is assumed (Table 1). This calculation assumes a random dipole orientation (κ^2 of $^2/_3$) for the coumarin and Trp34 dipoles which is probably a reasonable assessment based on discussions of the importance of κ^2 in monitoring distances using RET in biological systems (*33*). From anisotropy and

Table 1: RET Determination of the Distance from Trp34 to the Probe on CoumarinGb_3

protein tested	E (%)[a]	r (Å)[b]	limits (Å)[c]
VT1 B-subunit	98	13.3	11.8−14.8
VT1 holotoxin[d]	75	−	−

[a] E is resonance energy transfer efficiency. [b] r is the calculated distance between the probe on Gb_3 and Trp34 assuming random orientation. The R_0 for the Trp34/coumarinGb_3 pair is 25.4 Å based on an average Trp34 quantum yield of 0.23. [c] The half-height limits of distance were calculated by the method of Haas and co-workers (*31*), with polarization values of 0.20 for coumarinGb_3 and 0.30 for Trp34. [d] No distance was calculated between the fluorescent probes and the tryptophan residues on VT1 holotoxin due to the presence of two additional tryptophan residues on the A-subunit.

polarization determinations, the calculated distance between the coumarin on Gb_3 and Trp34 has lower and upper half-height error limits (*30*) of 11.8 and 14.8 Å, respectively, when only a single distance is considered (Table 1). When the size and position of the coumarin probe on Gb_3 are considered, the data indicate that Gb_3 is bound relatively close to Trp34 of VT1B. Moreover, the fact that saturation of maximum RET efficiency is achieved at slightly less than a 2-fold excess of coumarinGb_3 suggests that a single site on VT1B is responsible for the binding of this fluorescent Gb_3 derivative (Figure 3A). In cannot be ruled out, however, that more than one site is being filled. Alternatively, the r value calculated here may be slightly off due to minor impurities in the protein preparations used. While the data from Figure 3B showing that the residual fluorescence remains shifted to the blue suggest this is not the case, this possibility cannot be ruled out.

When RET experiments were carried out using coumarin-Gb_3 and the VT1 holotoxin, a maximum RET efficiency of 75% was achieved at less than a 2-fold molar excess of coumarinGb_3 (Table 1). This observation is consistent with the large RET from Trp34 to coumarinGb_3 described above, except that the fluorescence contributed by the two tryptophan residues of the VT1 A-subunit becomes significant due to the quenching of the five Trp34 residues within VT1B following its saturation with coumarinGb_3. As anticipated, the VT1 holotoxin fluorescence emission maximum is shifted to 350 nm after saturation with coumarinGb3 due to quenching of the blue-shifted fluorescence of Trp34.

Modification of Gb_3 with Coumarin Influences Its Binding Properties with Other Verotoxins. Although it was anticipated that Gb_3 would preferentially bind to site I of VT1B based on previously published molecular models (*22*), the data presented in Table 1 appear to be more consistent with site II binding. It should be noted, however, that lipid-free forms of Gb_3 bind weakly or not at all to VT1 (*40, 41*), suggesting that the lipid moiety greatly influences the manner in which the oligosaccharide is presented for toxin binding. It is therefore possible that the coumarin bound to Gb_3 may lead to the formation of a conformer that preferentially fits into site II.

To test this possibility, native Gb_3 and its coumarin-modified derivative were compared side-by side for their binding to VT1 and VT2c (Figure 4). Although each toxin type normally associates with Gb_3 receptors, VT1 binds much more tightly to Gb_3 than does VT2c, which accounts for the reduced cytotoxicity of the latter (*17*). However, while VT1

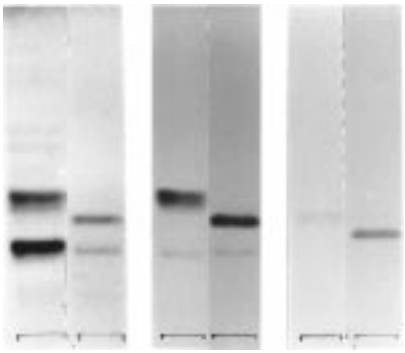

FIGURE 4: Thin-layer chromatography overlay analysis of the binding of VT1 and VT2c to Gb_3 and coumarinGb_3. For each pair of lanes, the left lane contains a mixture of Gb_3 (upper band) and Gb_4 (lower band), and the right lane contains coumarinGb_3. The minor band seen in the coumarinGb_3 lane is a small amount of unreacted lysoGb_3. The left panel shows the TLC lanes after staining the carbohydrate moieties with orcinol. The center panel is an overlay with ^{125}I-labeled VT1 to look for specific binding by this toxin. The right panel is a similar overlay done with VT2c.

is proposed to strongly bind Gb_3 within site I, VT2c has been proposed to preferentially bind Gb_3 within site II (*22*). What makes the latter result interesting is the fact that in TLC overlay experiments, Gb_3 with its acyl group replaced with coumarin demonstrates improved binding by VT2c (Figure 4), suggesting that coumarinGb_3 is held in a conformation that is better suited to binding by this form of the toxin. In contrast, VT1 appears to bind Gb_3 and coumarinGb_3 equally well. These data support the proposal that coumarinGb_3 binding occurs within site II of VT1B, or within both sites I and II.

Effect of Gb_3 Binding on the Accessibility of Trp34 to Different Small Molecules. RET data suggest that Gb_3 binds to VT1B in the vicinity of Trp34. Such binding would explain the profound influence that Gb_3 binding has on the fluorescence properties of Trp34 (see Figure 2) and implies that Gb_3 binding should have an influence on interactions between Trp34 and small molecules present in the aqueous environment. To investigate this possibility, the influence of Gb_3 binding on the quenching of Trp34 fluorescence by the uncharged polar solute acrylamide was examined. Acrylamide quenching provides a simple but sensitive means for monitoring the exposure of tryptophans in proteins to the surrounding solution (*42*, *43*). These quenching experiments were then extended to monitor the impact of Gb_3 binding on the quenching of Trp34 fluorescence by anionic and cationic agents.

After titrating VT1B with increasing concentrations of acrylamide in the presence or absence of Gb_3, acrylamide quenching of Trp34 fluorescence (expressed as F_0/F) was plotted as a function of acrylamide concentration. Upon examination of the resulting Stern−Volmer plots (Figure 5A), it becomes evident that both dynamic and static processes are at work in the quenching of Trp34 fluorescence in the absence of Gb_3. This combination of quenching processes results in an upward curve in the plot; however, after binding Gb_3, the Stern−Volmer plot for acrylamide quenching becomes linear (Figure 5A), suggesting that association with Gb_3 eliminates the static component of Trp34 quenching by this small polar agent. A similar observation was made for shiga toxin in the presence and absence of Gb_3 (*39*).

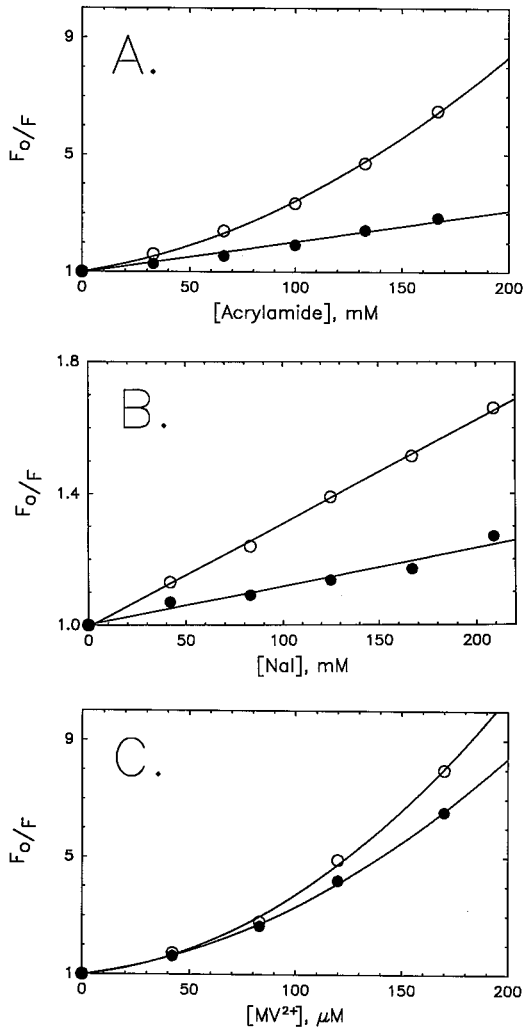

FIGURE 5: Quenching of Trp34 fluorescence in the absence (open symbols) and presence (closed symbols) of Gb_3. In (A), VT1B monomers (0.5 μM) were quenched with acrylamide in the absence or presence of 1 μM Gb_3; in (B), the same experiment was carried out for iodide quenching; and in (C), the same experiment was carried out for MV^{2+} quenching. Trp34 was excited at 282 nm, and fluorescence intensity was measured at 355 nm in the absence of Gb_3 or at 349 nm in the presence of Gb_3.

After determining the K_{SV} for acrylamide quenching from the initial slope of each plot, it appears that Gb_3 binding causes a slight decrease in acrylamide accessibility to Trp34 (Table 2). When the fluorescence lifetime of Trp34 is taken into account, the majority of this decreased accessibility appears to be due to the loss of the static component seen in the absence of Gb_3. In fact, the magnitude of the decrease in Trp34 fluorescence lifetime seen upon Gb_3 binding to VT1B (from 3.56 to 2.52 ns) relative to the decrease in acrylamide quenching could suggest that Trp34 actually becomes more accessible to the solvent upon lipid binding. In any case, it is clear that Gb_3 binding does influence the ability of acrylamide to quench Trp34 fluorescence, but it does not block solvent access to this residue.

To use fluorescence quenching as a tool for determining the effects of Gb_3 binding on the Trp34 microenvironment, iodide and methyl viologen (MV^{2+}) were used as negatively and positively charged quenching agents, respectively. In Table 2, Gb_3 binding was found to significantly decrease the K_{SV} for iodide quenching of Trp34 fluorescence, suggesting that formation of the Gb_3−VT1B complex protects

Table 2: Effect of Gb_3 Binding on Acrylamide, Iodide, and MV^{2+} Quenching of Trp34 Fluorescence[a]

quenching agent	Stern−Volmer quenching constant (K_{SV}), M^{-1}	
	$-Gb_3$	$+Gb_3$
acrylamide	11.6	10.5
iodide	3.15	1.17
MV^{2+}	712	924

[a] The quenching of Trp34 fluorescence in the absence and presence of Gb_3 was done as described under Materials and Methods. The values shown are the Stern−Volmer steady-state quenching constants (K_{SV}) which were derived from the slope of plots of F_0/F versus the concentration of quenching agent for each of the compounds listed. VT1B monomers were used at a concentration of 0.5 μM, and Gb_3 was used at 1 μM. Trp34 was excited at 282 nm, and fluorescence intensity was measured at 353 nm in the absence of Gb_3 and at 349 nm in the presence of Gb_3.

Table 3: Theoretical Distances from the Coumarin Attached to Gb_3 to All Five Trp34 Residues within the CoumarinGb_3−VT1B Complex

	model-based distance (Å)[a]		cocrystal distance (Å)[b]		
Trp34 residue[c]	site I	site II	site I	site II	site III
1	22.3	18.8	23.3	22.6	14.4
2	28.7	23.8	27.2	26.0	14.4
3	28.8	24.4	33.9	33.3	18.1
4	36.2	31.0	38.1	37.3	18.3
5	37.0	32.3	41.3	40.7	20.4

[a] These distances are from C1 of the acyl group of Gb_3 to C_γ of each Trp34 residue within the VT1B pentamer based on previously published models (*22*, *23*). [b] Distances within the cocrystals of VT1B and Pk-MCO (*25*) are from the glucose C1 of Pk-MCO to C_α of each Trp34 residue within the VT1B pentamer. [c] The distances given are listed from the shortest to longest which does not represent the order of the monomers around the VT1B pentameric ring structure.

Trp34 from collision and may result in an increase in negative charge in the vicinity of the tryptophan. Moreover, the absence of a curve in the quenching of Trp34 by iodide in the presence or absence of Gb_3 suggests there is no static quenching component in either case for this negatively charged quenching agent. This observation would be consistent with the Trp34 microenvironment possessing a negative charge that prevents the formation of ground-state complexes with anionic quenching agents. This local negative charge may be enhanced by Gb_3 binding, which results in a 65% decrease in the K_{SV} for iodide quenching of Trp34 fluorescence (Figure 5B).

Quenching data using MV^{2+} support the possibility that Trp34 is surrounded by negative charge that is increased by the binding of Gb_3. The presence of negative charge would explain why quenching of Trp34 fluorescence by MV^{2+} results in an upwardly curved Stern−Volmer plot (Figure 5C). The introduction of additional negative charge by Gb_3 binding would then explain why this upward curve is not eliminated as it is in the case of acrylamide quenching. Moreover, Gb_3 binding actually causes an apparent increase in MV^{2+} quenching of Trp34 fluorescence (Table 2) accompanied by an enhancement of the upward curve for MV^{2+} quenching (Figure 5). This increase in quenching is even more significant than is immediately apparent when it is taken into account that Gb_3 binding appears to cause a decrease in the Trp34 fluorescence lifetime. The upward curve for MV^{2+} quenching, together with the absence of a curve in the Stern−Volmer plots for iodide quenching, suggests that the protein region around Trp34 possesses a small amount of negative charge which is enhanced by VT1B binding of Gb_3. These data are consistent with previously described molecular models of VT1 binding to Gb_3 (*22*).

DISCUSSION

Verotoxin binding to Gb_3 receptors on endothelial cells is an essential step in the vascular pathology of hemorrhagic colitis and HUS. A great deal of effort has been directed at understanding the receptor−ligand interactions that mediate verotoxin action. It has been proposed that oral administration of matrix-bound Gb_3 oligosaccharide could provide a novel means of reducing the severity of HUS symptoms by competitively blocking toxin translocation into the circulatory system (*44*). Related to this, models for the interaction between VT1 and Gb_3 have provided an important foundation for the rational design of high-affinity soluble inhibitors with a variety of therapeutic potentials. In the present study, proposed models of Gb_3 binding to VT1B were tested using fluorescence spectroscopy as a tool for determining the distance from Trp34 of VT1B to a coumarin probe covalently linked to the site of fatty acid attachment on Gb_3.

Based on molecular models, there appear to be two sites on each VT1B monomer which are capable of accommodating Gb_3 binding (*22*, *23*). Binding of coumarinGb_3 at site I would place the γ-carbon of the Trp34 donor 22.3 Å from the probe on the nearest coumarin acceptor while binding at site II would place the γ-carbon of the Trp34 donor 18.8 Å from the nearest coumarin acceptor (*22*, *23*). Meanwhile, RET-based distance calculations indicate that the probe on coumarinGb_3 is located 13.3 Å from Trp34 on VT1B when a single distance is assumed (Table 1). It is important to realize, however, that Trp34 excitation energy can be donated to each of the five coumarinGb_3 molecules that are associated with the VT1B pentamer.

It has been suggested that a different sugar conformer binds into each predicted Gb_3 binding site and that lipid composition may affect the equilibrium between possible sugar conformers (*23*). This means that coumarinGb_3 may favor adopting a single sugar conformation and thus preferentially bind to either site I or site II, but probably not to both sites. With this in mind, coumarinGb_3 appears to bind to site II because when the distances from Trp34 to all available coumarinGb_3 acceptors are taken into account (given in Table 3), a theoretical RET of 98.5% would be predicted. From eq 2, this would give an apparent single distance of 12.6 Å, which compares favorably with the observed distance calculated using RET of 13.3 Å with upper and lower limits of 14.8 and 11.8 Å, respectively. If site I was occupied, a RET efficiency near 88.3% would be predicted for energy transfer to all five coumarinGb_3 acceptors. This would give an apparent single distance of 18.1 Å, which does not compare as well with the apparent distance of 13.3 Å calculated here. Alternatively, if both sites I and II were occupied by coumarinGb_3, a total RET efficiency of 99.8% would be expected which would give a single apparent distance of 9.0 Å. This is certainly a possibility but is not consistent with the fact that maximum RET efficiency is approached at a coumarinGb_3 to VT1B monomer ratio of less than 2.

Recently, the crystal structure of VT1B complexed with Pk-MCO was reported at 2.8 Å resolution with three potential Gb_3 binding sites described (*25*). The first of these sites corresponds roughly with site I identified using molecular models (*22*, *23*) while the second corresponds to the previously proposed site II except that the orientation of the Gb_3 trisaccharide moiety is different within the VT1B cleft site (*22*, *23*, *25*). The significance of the latter observation is that the distance separating the ceramide attachment site of Gb_3 and Trp34 on VT1B would be different for each site II orientation. Based on the published structure of the VT1B/Pk-MCO cocrystal, the position of the C1 carbon of the glucose on Gb_3 (which is slightly closer to Trp34 than would be the site occupied by the acceptor on coumarinGb_3) is 22.6 Å from the C_α of Trp34. When considering the distances from the Trp34 C_α position to each glucose C1 carbon on Pk-MCO when all five Gb_3 binding sites on VT1B are filled, a RET efficiency of less than 87% would be obtained which does not fit with the spectroscopic data observed here.

Interestingly, Ling and co-workers (*25*) also describe a third binding site for Pk-MCO in which the C1 of glucose is located extremely close to the C_α of Trp34 (see Table 3). Occupation of site III by coumarinGb_3 for the VT1B pentamer would result in an energy transfer efficiency of 100%. While site III binding could explain the high degree of RET efficiency described here, there are no other data to corroborate the existence of this binding site (*25, 36*), and mutagenesis studies have shown that Trp34 is not essential for cytotoxicity (*37*). Moreover, dynamic quenching of Trp34 fluorescence by acrylamide is not eliminated by Gb_3 binding, suggesting that lipid binding by VT1B does not limit the access of small uncharged solutes to Trp34 as might be expected if site III binding had occurred.

It is possible that the discrepancy between crystallographic analyses and model-based predictions is a result of the nature of the hydrophobic group to which the Gb_3 trisaccharide is attached. As already mentioned, the structure of the lipid moiety of Gb_3 can have a profound impact on the nature of the interaction between this glycolipid and VT1 (*23*). Replacement of the entire ceramide moiety of Gb_3 with the methoxycarbonyl group used in cocrystal formation (and the absence of an associated phospholipid membrane) could greatly influence the way in which the trisaccharide portion of Gb_3 fits into the cleft site of VT1B. In this respect, the data presented here may represent a more physiologically relevant association between VT1B and Gb_3 than does the formation of cocrystals from VT1B and soluble Pk-MCO.

In addition to using RET to monitor the position of coumarinGb_3 binding on VT1B, fluorescence quenching experiments were used to monitor the effect Gb_3 binding has on the Trp34 microenvironment. Interestingly, acrylamide appears to quench the fluorescence of Trp34 by both static and dynamic mechanisms in the absence of Gb_3 but by only a single (probably dynamic) mechanism in VT1B/Gb_3 complexes. The data suggest that Gb_3 binding displaces an acrylamide binding site near Trp34 which is responsible for static quenching of tryptophan fluorescence. However, acrylamide does not limit the exposure of Trp34 to soluble acrylamide, suggesting that Gb_3 binding to VT1B does not involve intimate contact between the lipid and Trp34. This would be consistent with site I or II binding in which direct contact between Gb_3 and Trp34 is not anticipated, but would argue against the occurrence of site III binding which would be anticipated to greatly reduce the dynamic component of Trp34 fluorescence quenching by acrylamide.

In contrast to quenching by acrylamide, a single quenching mechanism appears to be at work in the quenching of Trp34 fluorescence by iodide as indicated by the linear Stern−Volmer plots in the presence and absence of Gb_3. This may indicate that there is a net negative charge in the vicinity of Trp34 that prevents iodide from establishing a static quenching component. This conclusion is supported by the results of quenching experiments using MV^{2+} which show that both dynamic and static processes are at work in the quenching of Trp34 fluorescence by this divalent cation whether Gb_3 is present or not. Moreover, the large degree of protection of Trp34 from iodide quenching following VT1B association with Gb_3 suggests that lipid binding contributes additional negative charge to the vicinity of Trp34. This is supported by the absence of any protection of Trp34 from MV^{2+} following Gb_3 binding and is consistent with the proposal that the region around Trp34 has an overall negative charge, which becomes even more negatively charged upon VT1B association with Gb_3. This is also consistent with the binding of Gb_3 within the cleft of VT1B as hypothesized in previously proposed models of VT1B binding to its Gb_3 receptor (*23*).

Here we report experimental data that complement previous model-based predictions on the binding of Gb_3 to the B-subunit of VT1. This information will be useful in assessing the accuracy of predicted models for various Gb_3 binding sites on VT1. Moreover, this study underscores the importance of using fluorescence spectroscopy, in conjunction with molecular modeling, crystallographic data, and biochemical analyses, as an important part of future structure-based drug design research aimed at preventing and treating HUS and related vascular pathologies.

ACKNOWLEDGMENT

We gratefully acknowledge fluorescence lifetime analyses performed by D. Thompson (The Johns Hopkins University, Baltimore, MD) in the laboratory of J. Petersen (Wayne State University, Detroit, MI). We also thank P.-G. Nyholm for the distances derived from models of the docking of Gb_3 into the cleft site of VT1B.

REFERENCES

1. Endo, Y., Tsurugi, K., Yutsudo, T., Takeda, Y., Ogasawara, T., and Igarashi, K. (1988) *Eur. J. Biochem. 17*, 45−50.
2. Ramotar, K., Boyd, B., Tyrrell, G., Gariepy, J., Lindwood, C., and Brunton, J. (1990) *Biochem. J. 272*, 805−811.
3. Lingwood, C. A. (1993) *Adv. Lipid Res. 25*, 189−212.
4. Karmali, M. A. (1989) *Clin. Microbiol. Rev. 2*, 15−38.
5. Lingwood, C. A. (1994) *Nephron 66*, 21−28.
6. Taylor, C. M. (1995) *J. Infect. 30*, 189−192.
7. Obrig, T. G., Del Vecchio, P. J., Brown, J. E., Moran, T. P., Rowland, B. M., Judge, T. K., and Rothman, S. W. (1988) *Infect. Immun. 56*, 2373−2378.
8. Obrig, T., Louise, C. B., Lingwood, C. A., Boyd, B., Barley-Maloney, L., and Daniel, T. O. (1993) *J. Biol. Chem. 268*, 15484−15488.
9. Louise, C. B., and Obrig, T. G. (1991) *Infect. Immun. 59*, 4173−4179.
10. Louise, C. B., and Obrig, T. G. (1992) *Infect. Immun. 60*, 1536−1543.

11. Mangeney, M., Richard, Y., Coulaud, D., Tursz, T., and Wiels, J. (1991) *Eur. J. Immunol. 21*, 1131−1140.
12. Gregory, C. D., Tursz, T., Edwards, C. F., Tetaud, C., Talbot, M., Caillou, B., Rickinson, A. B., and Lipinski, M. (1987) *J. Immunol. 139*, 313−318.
13. Cohen, A., Hannigan, G. E., Williams, B. R. G., and Lingwood, C. A. (1987) *J. Biol. Chem. 262*, 17088−17099.
14. Lingwood, C. A., and Yiu, S. C. K. (1992) *Biochem. J. 283*, 25−26.
15. Ghislain, J., Lingwood, C. A., and Fish, E. N. (1994) *J. Immunol. 153*, 3655−3663.
16. Maloney, M. D., and Lingwood, C. A. (1994) *J. Exp. Med. 180*, 191−201.
17. Lingwood, C. A. (1996) *Trends Microbiol. 4*, 147−153.
18. Lingwood, C. A. (1996) *Glycoconjugate J. 13*, 495−503.
19. Mangeney, M., Lingwood, C. A., Taga, S., Caillou, B., Tursz, T., and Wiels, J. (1993) *Cancer Res. 53*, 5314−5319.
20. Cohen, A., Madrid-Marina, V., Estrov, Z., Freedman, M. H., Lingwood, C. A., and Dosch, H. M. (1990) *Int. Immunol. 2*, 1−8.
21. Farkas-Himsley, H., Hill, R., Rosen, B., Arab, S., and Lingwood, C. A. (1995) *Proc. Natl. Acad. Sci. U.S.A. 92*, 6996−7000.
22. Nyholm, P., Magnusson, G., Zheng, Z., Norel, R., Binnington-Boyd, B., and Lingwood, C. A. (1996) *Chem. Biol. 3*, 263−275.
23. Nyholm, P.-G., Brunton, J. L., and Lingwood, C. A. (1996) *Int. J. Biol. Macromol. 17*, 199−205.
24. Stein, P. E., Boodhoo, A., Tyrrell, G. J., Brunton, J. L., and Read, R. J. (1992) *Nature (London) 355*, 748−750.
25. Ling, H., Boodhoo, A., Hazes, B., Cummings, M. D., Armstrong, G. D., Brunton, J. L., and Read, R. J. (1998) *Biochemistry 37*, 1777−1788.
26. De Grandis, S., Ginsberg, J., Toone, M., Climie, S., Friesen, J., and Brunton, J. (1987) *J. Bacteriol. 169*, 4313−4319.
27. Kiarash, A., Boyd, B., and Lingwood, C. A. (1994) *J. Biol. Chem. 269*, 11138−11146.
28. McCann, J. A., Mertz, J. A., Czworkowski, J., and Picking, W. D. (1997) *Biochemistry 36*, 9169−9178.
29. Lakowicz, J. R. (1983) *Principles of Fluorescence Spectroscopy*, Plenum Press, New York.
30. Stryer, L. (1978) *Annu. Rev. Biochem. 47*, 819−846.
31. Haas, E., Katchalski-Katzir, E., and Steinberg, I. Z. (1978) *Biochemistry 17*, 5064−5070.
32. Wu, P., and Brand, L. (1994) *Anal. Biochem. 218*, 1−13.
33. dos Remedios, C. G., and Moens, P. D. J. (1995) *J. Struct. Biol. 115*, 175−185.
34. Odom, O. W., Robbins, D. J., Lynch, J., Dottavio-Martin, D., Kramer, G., and Hardesty, B. (1980) *Biochemistry 19*, 5947−5954.
35. Highsmith, S., and Murphy, A. J. (1984) *J. Biol. Chem. 259*, 14651−14656.
36. Richardson, J. M., Evans, P. D., Homans, S. W., and Donohue-Rolfe, A. (1997) *Nat. Struct. Biol. 4*, 190−193.
37. Jemal, C., Haddad, J. E., Begum, D., and Jackson, M. P. (1995) *J. Bacteriol. 177*, 3128−3132.
38. Stern, D., and Volmer, M. (1919) *Phys. Z. 20*, 183−188.
39. Surewicz, W. K., Surewicz, K., Mantsch, H. H., and Auclair, F. (1989) *Biochem. Biophys. Res. Commun. 160*, 126−132.
40. Boyd, B., Zhiuyan Z., Magnusson, G., and Lingwood, C. A. (1994) *Eur. J. Biochem. 223*, 873−878.
41. St. Hilaire, P. M., Boyd, M. K., and Toone, E. J. (1994) *Biochemistry 33*, 14452−14463.
42. Efting, M. R., and Ghiron, C. A. (1981) *Anal. Biochem. 114*, 199−227.
43. DeWolf, M. J. S., Fridkin, M., Epstein, M., and Kohn, L. D. (1981) *J. Biol. Chem. 256*, 5481−5488.
44. Armstrong, G. D., Fodor, E., and Vanmaele, R. (1991) *J. Infect. Dis. 164*, 1160−1167.

BI982335N